Magnetic Resonance Imaging 63 (2019) 250–257

Contents lists available at ScienceDirect

Magnetic Resonance Imaging

journal homepage: www.elsevier.com/locate/mri

Original contribution

Noise estimation for the velocity in MRI phase-contrast

Pablo Irarrazaval[a,b,c,d,*], Ali Dehghan Firoozabadi[e], Sergio Uribe[b,d,f], Cristian Tejos[a,b], Carlos Sing-Long[b,c,g]

[a] Electrical Engineering Department, Pontificia Universidad Catolica de Chile, Santiago 7820436, Chile
[b] Biomedical Imaging Center, Pontificia Universidad Catolica de Chile, Santiago 7820436, Chile
[c] Institute for Biological and Medical Engineering, Pontificia Universidad Catolica de Chile, Santiago 7820436, Chile
[d] Millennium Nucleus for Cardiovascular Magnetic Resonance, Santiago, Chile
[e] Department of Electricity, Universidad Tecnologica Metropolitana, Av. Jose Pedro Alessandri 1242, 7800002 Santiago, Chile
[f] Radiology Department, School of Medicine, Pontificia Universidad Catolica de Chile, Santiago 7820436, Chile
[g] Institute for Mathematical and Computational Engineering, Pontificia Universidad Catolica de Chile, Santiago 7820436, Chile

ARTICLE INFO

Keywords:
Flow MRI
Phase contrast velocity
Velocity-to-Noise Ratio

ABSTRACT

The purpose of this study is to estimate the precision or statistical variability of the velocity measurements computed from MRI phase-contrast. From the analytical probability density function (PDF) of the phase in the signal we obtain the PDF of the velocity by means of an auto-convolution. This PDF allows the estimation of the precision of the velocity, important for the correct interpretation of the many parameters that are based on it. We show that for high Signal-to-Noise Ratio (SNR) voxels, the distribution is well approximated by a Gaussian distribution. On the other hand, this is not true for lower SNR voxels, where the distribution adopts a form in between the Gaussian and the uniform distributions. This was confirmed empirically. Also, knowing the PDF on a coil by coil basis it is possible to combine the data from multiple coils in an optimal way. We showed that the optimal combination reduces the resulting global variability of the velocity, in comparison with the commonly used Weighted Mean or with a SENSE reconstruction with R = 1.

1. Introduction

MRI phase-contrast [1] is a well known technique used to compute the velocity associated to each pixel. It assumes that all spins within the pixel have the same velocity (equivalently, it measures an average velocity) and that it is constant during the readout. These velocities are used in many applications such as MRI-PC Angiography [2], 4D Flow [3], quantization flow-rate [4], wall shear stress [5, 6], pressure [7, 8], and others.

For many of these applications, it is necessary to quantify the precision or statistical variation and the accuracy or statistical bias of the measured velocity. For example, when 4D Flow velocities are used to feed a fluid mechanic model to estimate physiologically important parameters, such as pressure. In order to characterize the variability of these parameters, it is necessary to know the variability of the velocity as an important input to the model. The accuracy of the velocity is not a problem because its expected value does not change with the noise in the signal. In the case of partial volume, that value is the mean velocity within the voxel.

In most of the literature referring to the Velocity-to-Noise Ratio (VNR) [9-12], it is assumed that the standard deviation of the velocity is:

$$\sigma_V = \frac{\sqrt{2}}{\pi}\frac{V_{\text{enc}}}{\text{SNR}} \tag{1}$$

where V_{enc} is the maximum encoded velocity and SNR, the signal-to-noise ratio in the image. We will show that this is not necessarily true, firstly, because the standard deviation is not the same for all pixels as stated in Refs. [13] and [14], and secondly, because this formula assumes a Gaussian distribution in the velocity which is not valid for low signal regions [15].

The purpose of this study is to state the exact probability distribution function (PDF) of the error in the velocity, and to promote its use to describe its precision, particularly in low SNR regions [16]. We provide a simple graph from where the velocity standard deviation can be estimated. We also propose to use these standard deviations to combine the velocity measured from multiple coils with the purpose of reducing the total combined variance.

To confirm the theoretical results, we measured the velocity several times in a simple flow phantom and compared the empirical histogram

* Corresponding author at: Pontificia Universidad Catolica de Chile, Santiago 7820436, Chile.
E-mail address: pim@uc.cl (P. Irarrazaval).

https://doi.org/10.1016/j.mri.2019.08.028
Received 4 January 2019; Received in revised form 1 August 2019; Accepted 15 August 2019

with the theoretical PDF. We also applied our methodology to the velocity acquired from the ascending and descending aorta of a volunteer using a standard protocol for 4D Flow. Finally, we show how the more correct standard deviations can be used to combine the data from multiple coils.

In this study, we present the true PDF for the velocity and how it can be used to combine the velocity from multiple coils in an optimal sense. With phantom experiments, we validate this PDF and with in-vivo data, we show that our method for combining the velocity obtained from multiple coils produced more precise velocities.

2. MRI phase-contrast

For simplicity of notation, we will assume two acquisitions, one without velocity encoding M_o, and another with velocity encoding M_1. In practice, there may be more encodings and they may occur in other combinations, but the principles are the same. $\mathbf{k}_v$ is the first moment of the gradients. It is assumed that $\mathbf{k}_v$ is constant during the readout and it is given exclusively by the first moment of the encoding bipolar gradient:

$$\mathbf{k}_v = \frac{\gamma}{2\pi}\int \tau \mathbf{G}_{\text{enc}}(\tau)d\tau \tag{2}$$

It is also assumed that the velocity $\mathbf{v}(\mathbf{x})$ is unique for each pixel $\mathbf{x}$ and constant in time.

In a noiseless situation, the two reconstructed images would be:

$$\begin{aligned} \mathrm{m}_0(\mathbf{x}) = \mathrm{m}(\mathbf{x}) &= |\mathrm{m}(\mathbf{x})|\, e^{i\phi_0(\mathbf{x})} \quad \text{and} \quad \mathrm{m}_1(\mathbf{x}) = \mathrm{m}(\mathbf{x})e^{-i2\pi\mathbf{k}_v v(\mathbf{x})} \\ &= |\mathrm{m}(\mathbf{x})|\, e^{i\phi_1(\mathbf{x})} \end{aligned} \tag{3}$$

where m_o and m_1 are the inverse Fourier Transform of M_o and M_1. The velocity is estimated as the difference of the phases:

$$2\pi\mathbf{k}_v\cdot\mathbf{v}(\mathbf{x}) = \phi_o(\mathbf{x}) - \phi_1(\mathbf{x}) = \Delta\phi(\mathbf{x}) \tag{4}$$

where ϕ and $\Delta\phi$ are in the range $-\pi\ldots\pi$.

Let $V\text{enc} = 1/(2|\mathbf{k}_v|)$ be the encoding velocity, $v(\mathbf{x}) = \hat{\mathbf{k}}_v\cdot\mathbf{v}(\mathbf{x})$, the projection of the velocity in the direction of the encoding, and $\hat{v}(\mathbf{x}) = v(\mathbf{x})/V\text{enc}$, the velocity in units of Venc, then:

$$\hat{v}(\mathbf{x}) = \frac{\Delta\phi(\mathbf{x})}{\pi}. \tag{5}$$

3. Material and methods

3.1. Effect of acquisition noise in the velocity

We assume that the signal acquisition has independent and identically distributed additive Gaussian noise in the real and imaginary channels of M_o and M_1. We are assuming that the noise is mostly dominated by thermal noise coming from the body, and we are not considering artifacts as part of the noise component. To compute the PDF of the velocity, we first derive the PDF of the phase $p_\Phi(\phi)$, and then we compute the auto-convolution (cyclically) to find the PDF of the velocity $p_{\Delta\Phi}(\Delta\phi)$. This is done in a per pixel basis, so we drop the dependence of $\mathbf{x}$.

We analyze the values of m_0 and m_1 as vectors in the complex plane. Without loss of generality, we assume that m_0 is real and of magnitude a, such that the measured values will follow a bi-dimensional Gaussian distribution centered in a with a standard deviation σ for the real and imaginary parts as shown in Fig. 1. This distribution of the noisy value is the same for all pixels, since it comes from the MR signal acquisition noise.

The probability distribution of the angle ϕ will be given by the line integral of the 2D distribution along the direction ϕ, starting from the origin. Let $p_{R,\Phi}(r,\phi)$ be the PDF of the noisy value in polar coordinates:

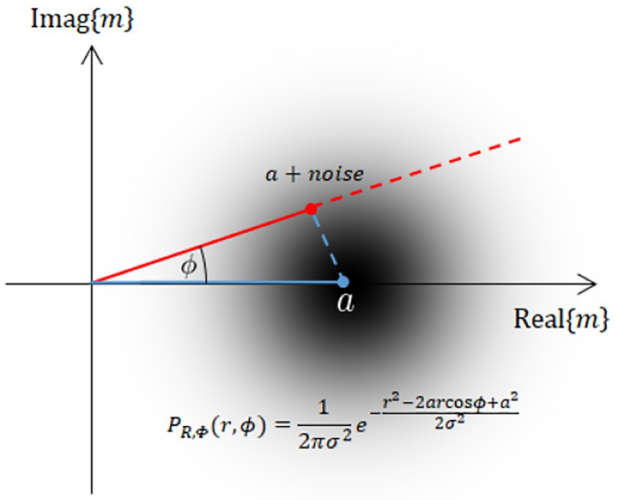

Fig. 1. Signal probability distribution in the complex plane from where it is possible to compute the probability of ϕ.

$$p_{R,\Phi}(r,\phi) = \frac{1}{2\pi\sigma^2}e^{-\frac{r^2-2ar\cos\phi+a^2}{2\sigma^2}} \tag{6}$$

The PDF of ϕ is then:

$$p_\Phi(\phi) = \frac{1}{2\pi\sigma^2}\int_0^\infty re^{-\frac{r^2-2ar\cos\phi+a^2}{2\sigma^2}}dr \tag{7}$$

which can be solved to be [17, 18]:

$$p_\Phi(\phi) = \frac{1}{2\pi}e^{-\frac{a^2}{2\sigma^2}}\left(1 + e^{\frac{a^2}{2\sigma^2}\cos^2\phi}\sqrt{\pi}\frac{a}{\sqrt{2}\sigma}\cos\phi\left(1+\mathrm{erf}\left(\frac{a}{\sqrt{2}\sigma}\cos\phi\right)\right)\right) \tag{8}$$

where erf is the error function. This expression is parameterized to the ratio (a/σ), a quantity related to the signal-to-noise ratio of the original signal but not exactly SNR since a is position dependent. To simplify notation, we define $b = \frac{1}{\sqrt{2}}(a/\sigma)$:

$$p_\Phi(\phi) = \frac{1}{2\pi}(e^{-b^2} + e^{-b^2\sin^2\phi}\sqrt{\pi}b\cos\phi(1+\mathrm{erf}(b\cos\phi))) \tag{9}$$

This PDF is plotted in Fig. 2a for different values of b.

For $b = 0$ (no signal) the probability is uniformly distributed in $-\pi\ldots\pi$, which can be easily verified in $p_\Phi(\phi)$ since $e^{-b^2} = 1$ and the second term is zero:

$$p_\Phi(\phi) = \frac{1}{2\pi} \tag{10}$$

For a greater b (more signal), the PDF tends towards a Gaussian distribution. This can be verified by noting $e^{-b^2} \approx 0$, $1 + \mathrm{erf}(b\cos\phi) \approx 2\sqcap\left(\frac{\phi}{\pi}\right)$, $\sin\phi \approx \phi$, and $\cos\phi \approx 1$ such that $e^{-b^2\sin^2\phi}\cos\phi \approx e^{-b^2\phi^2}$:

$$p_\Phi(\phi) \approx \frac{b}{\sqrt{\pi}}e^{-b^2\phi^2} \tag{11}$$

which is of course the Gaussian distribution:

$$p_\Phi(\phi) = \frac{1}{\sqrt{2\pi}\sigma_\phi}e^{-\phi^2/2\sigma_\phi^2} \tag{12}$$

with $\sigma_\phi = 1/(\sqrt{2}b) = \sigma/a$.

Finally, the probability distribution of the velocity (or phase difference) is the auto-convolution of the PDF in Eq. (12),

$$p_{\Delta\Phi}(\Delta\phi) = p_\Phi(\phi)^{\circledast}p_\Phi(\phi) \tag{13}$$

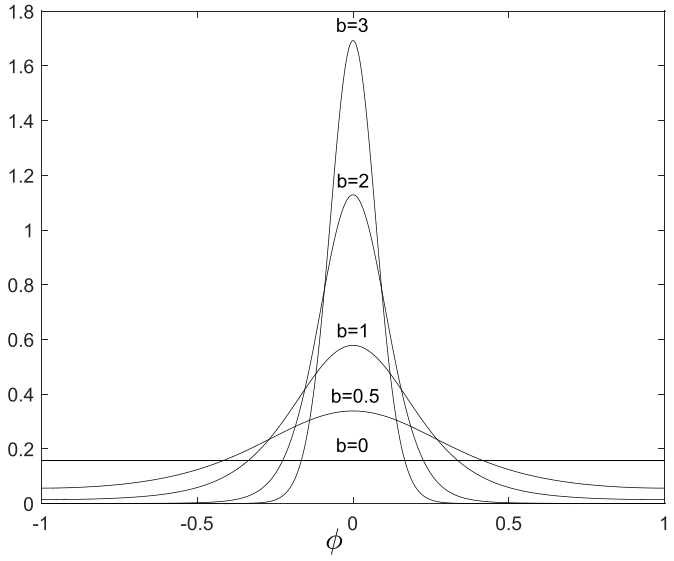

(a) PDF of ϕ

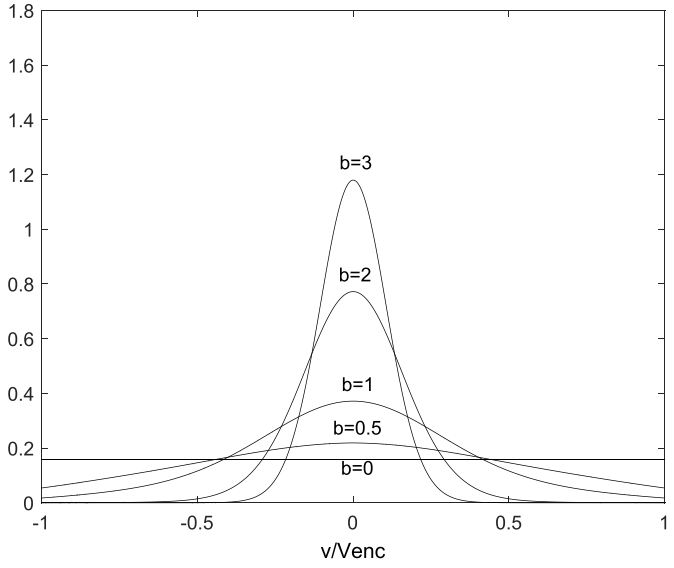

(b) PDF of the velocity ($\Delta\phi/\pi$)

Fig. 2. Probability distribution of ϕ and $\Delta\phi$ for different values of b.

where $\bar{*}$ is the periodic convolution in the interval $-\pi\ldots\pi$. The result of this convolution is shown in Fig. 2b for different values of b. We only plotted the case of mean velocity $\bar{v} = 0$. For other velocities, this PDF is trivially shifted to $\bar{v} = v - v_0$.

A more practical way for having a notion of the precision of the velocity is to look at its standard deviation and the 68% and 95% intervals (they would correspond to one and two standard deviations if the distribution were Normal). The standard deviation for each b value is shown in Fig. 3a and the intervals in Fig. 3b.

We will consider the Gaussian distribution as a good approximation for the PDF when the root mean square difference between the actual PDF and the Gaussian PDF is less than 1%. Given this definition, it can be noted that for b values less than 2.5, the Gaussian approximation fails, and the standard deviation is overestimated ($b < 0.7$) or slightly underestimated ($0.7 < b < 2.5$).

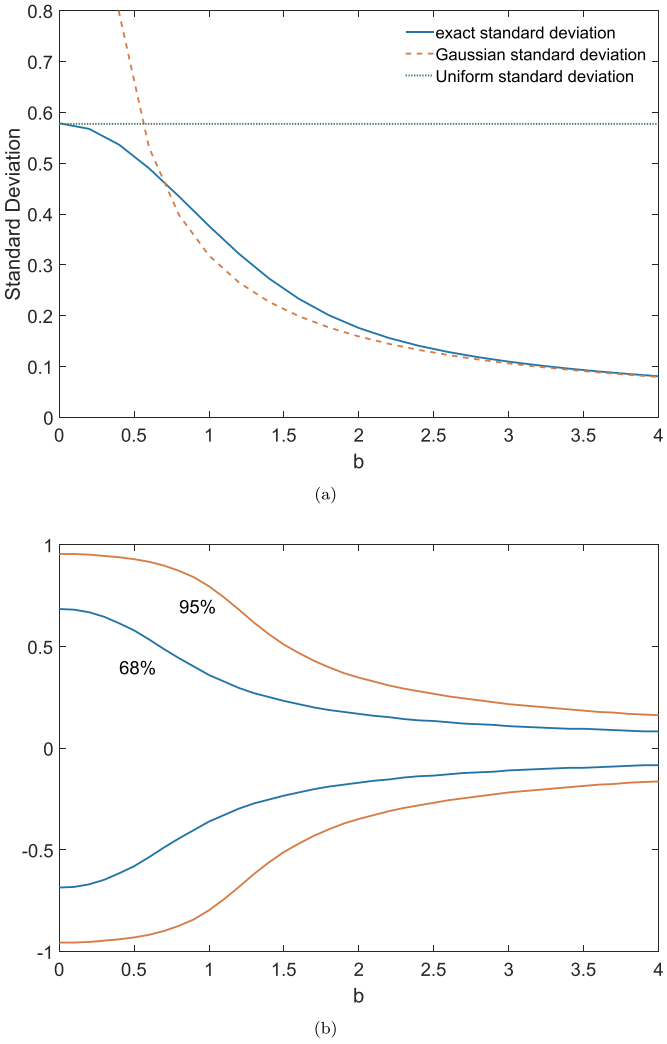

Fig. 3. a) Standard deviation of v/Venc and b) the 68% and 95% interval for v/Venc as a function of b. In (a), we also plot the standard deviation for the uniform and Gaussian distribution.

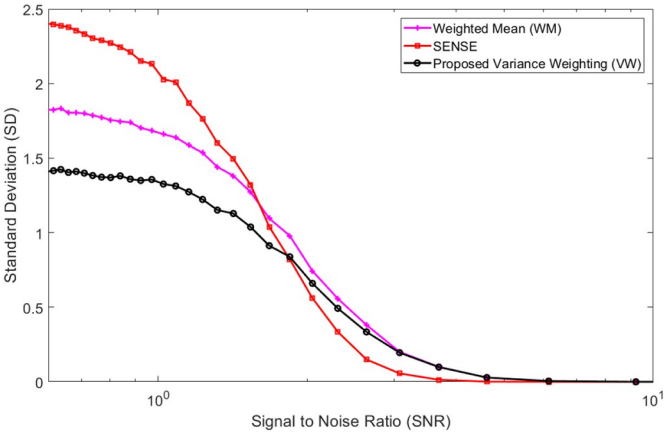

Fig. 4. Total Standard Deviation (SD) of the combined velocity for the three methods: Weighted Mean (WM), SENSE and the proposed combination with Variance Weighting (VW).

3.2. Multiple coils

In a realistic setting, it is common to have data from multiple coils. Combining multiple velocities measured by a phase-array coil is not

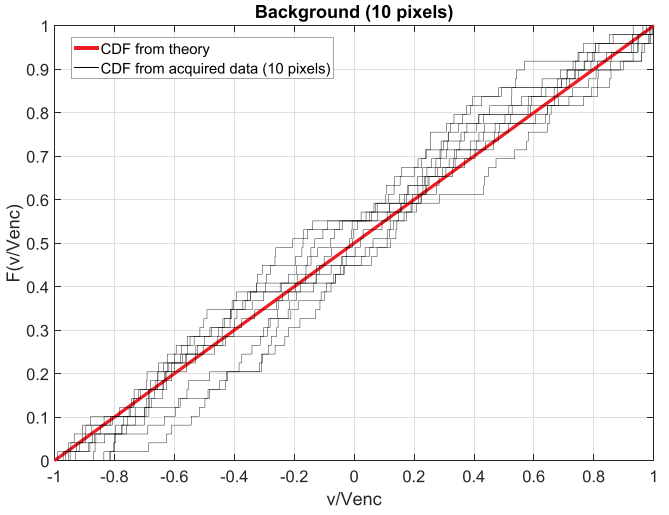

(a)

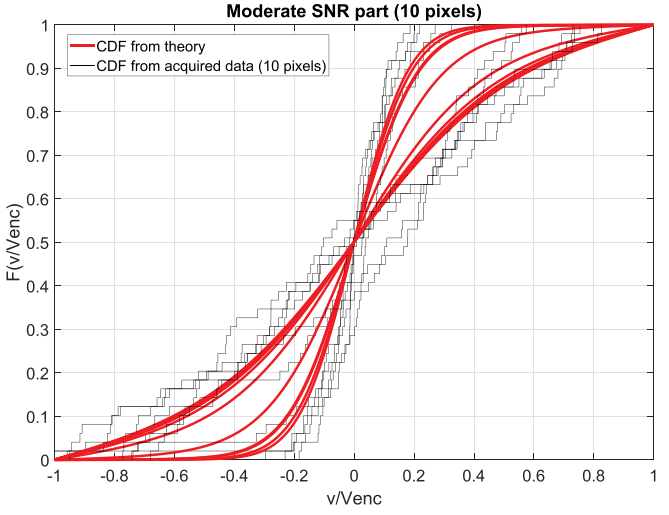

(b)

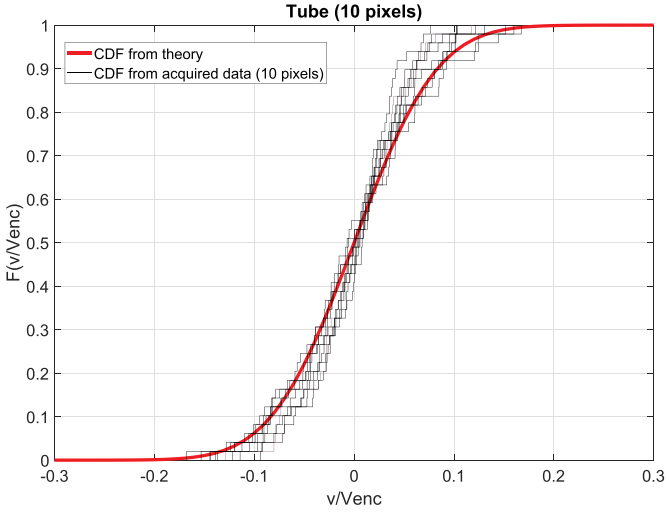

(c)

Fig. 5. Cumulative Distribution Functions (CDF) for three groups of pixels. a) CDF for 10 pixels in the background, low SNR ($b \approx 0$). b) CDF for 10 pixels in a moderate SNR region ($0.75 < b < 2.3$). And c) CDF for 10 pixels inside the tube, high SNR ($b > 2.3$). The solid red line indicates the theoretical values and shown in gray is the empirical histogram. (For interpretation of the references to color in this figure legend, the reader is referred to the web version of this article.)

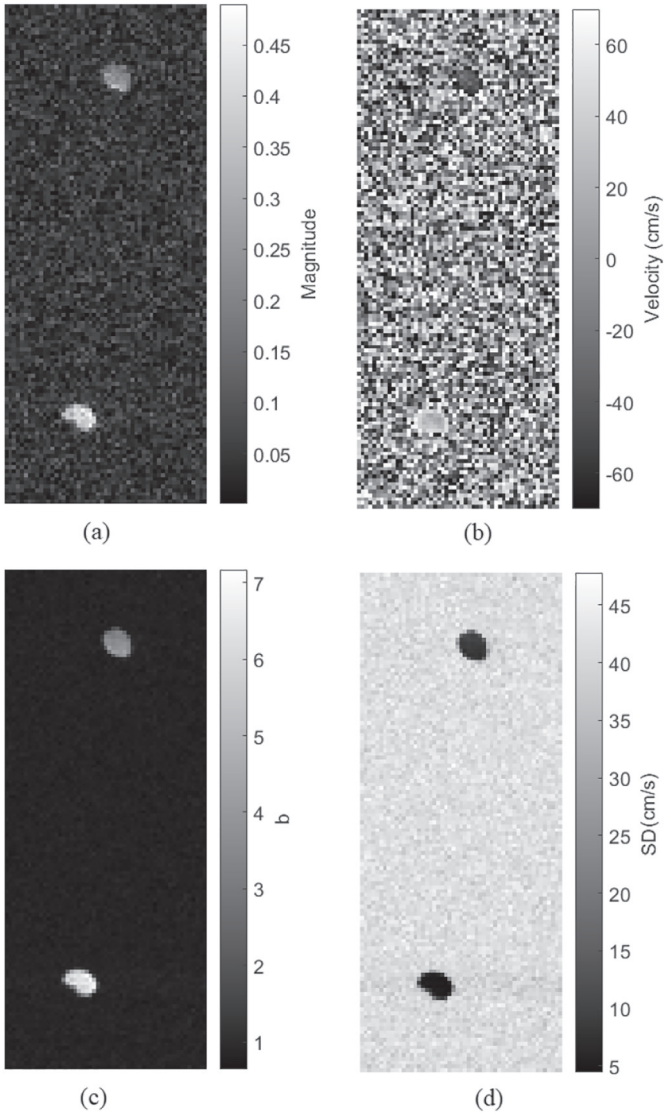

Fig. 6. Simple velocity phantom: In the top row, the magnitude (a) and velocity (b) images. In the bottom row, the b values (c) and the standard deviation (d).

trivial. Currently used methods include Weighted Mean (WM) whereby the phase (velocity) of a weighted sum of the complex images is used, and SENSE reconstruction [19-21], whereby the phase of an optimal coil-combined image is used. In this section, we propose a method for combining the multiple velocities to minimize the combined velocity variance.

The combined velocity of multiple coils can be expressed as:

$$v = \sum_i w_i v_i, \tag{14}$$

Such that the final PDF of the velocity is a repeated convolution:

$$p_V(v) = \frac{1}{w_1 \cdots w_N} p_{V_1}(v/w_1) \circledast \ldots \circledast p_{V_N}(v/w_N). \tag{15}$$

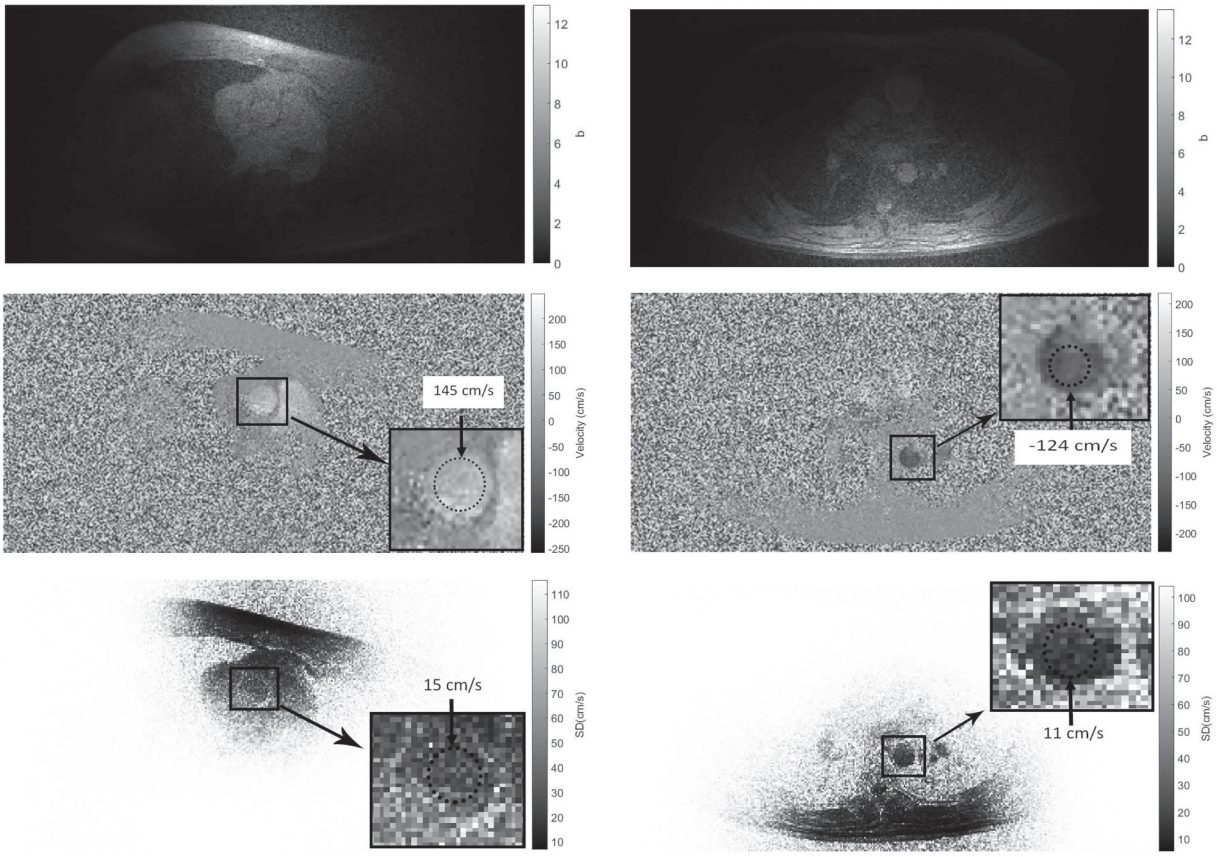

Fig. 7. Ascending (left) and descending (right) aorta for one particular time frame and one coil, parameter b (first row), velocity (second row) and velocity standard deviation (SD) (third row).

Typically, the weights w_i are computed to minimize the final velocity variance ($w = \arg\min \sum_i w_i^2 \sigma_{v_i}^2$). If the PDF of the velocity were Gaussian, these weights would depend only on the coil sensitivities and are [19, 22]:

$$w_i = \frac{S_i^2}{\sum_j S_j^2}. \tag{16}$$

But for arbitrary variances per coil, the weights that minimize the total variance are:

$$w_i = \frac{\prod_{j \neq i} \sigma_{v_j}^2}{\sum_k \prod_{j \neq k} \sigma_{v_j}^2}. \tag{17}$$

For instance, for 3 coils the weights are:

$$w_1 = \frac{\sigma_{v_2}^2 \sigma_{v_3}^2}{D} \qquad w_2 = \frac{\sigma_{v_1}^2 \sigma_{v_3}^2}{D} \qquad w_3 = \frac{\sigma_{v_1}^2 \sigma_{v_2}^2}{D} \tag{18}$$

with $D = \sigma_{v_2}^2 \sigma_{v_3}^2 + \sigma_{v_1}^2 \sigma_{v_3}^2 + \sigma_{v_1}^2 \sigma_{v_2}^2$. We will call this "Variance Weighting" (VW).

To compute the weights, we propose using the actual variance as shown in Fig. 3a. To estimate the magnitude of the image, a, we use the weighted average of the coils as an approximation.

$$a_i = S_i \left| \sum_k S_k m_k \right| \tag{19}$$

where m_i are the complex images and S_i are the coil sensitivities. The sensitivities can be estimated from the same images using low-pass filtering. The signal standard deviation, σ_i can be estimated from background pixels, since it is the same for all pixels, taking care of choosing an artifact free region.

For comparison purposes, in our Fig. 4, we recreated Figure 1 from Ref. [20]. We added our proposed combination method to the two methods shown in Ref. [20] (WM and SENSE) and we also extend the analysis to lower SNR (SNR from 1 to 10 as opposed to from 3 to 10) where our method makes the most difference. As can be readily seen, the total variance is significantly reduced for low SNR situations. As expected, for higher SNR values there is not much difference.

3.3. Experiments

To test the theoretical analysis, we performed two experiments, in a velocity phantom and on one volunteer. The velocity phantom consisted of a vinyl tubing circuit (12 mm diameter) connected to a water pump which produced a constant water flow of approximately 2.4 l/min and T1 = 4000 ms. The acquisition was done in a 1.5 T Philips Achieva scanner employing a 2D Fast Field Echo sequence with TR/TE = 7.1/4.1 ms, resolution of 1.5 × 1.5 × 4mm^3 and a Venc = 70 cm/s in the through plane direction employing a surface coil. The acquisition was repeated 50 times (with and without velocity encoding) and under the exact same conditions. We computed the parameter a as the pixel magnitude averaged over the 50 acquisitions and, σ of the noise as the standard deviation of the real and imaginary components of the signal for the 50 acquisitions.

We also illustrate the application of our analysis for one volunteer. We separately scanned the ascending and descending aorta to ensure an anatomically perpendicular plane at each location. It was acquired in the same Philips scanner with a five-element cardiac coil, employing a

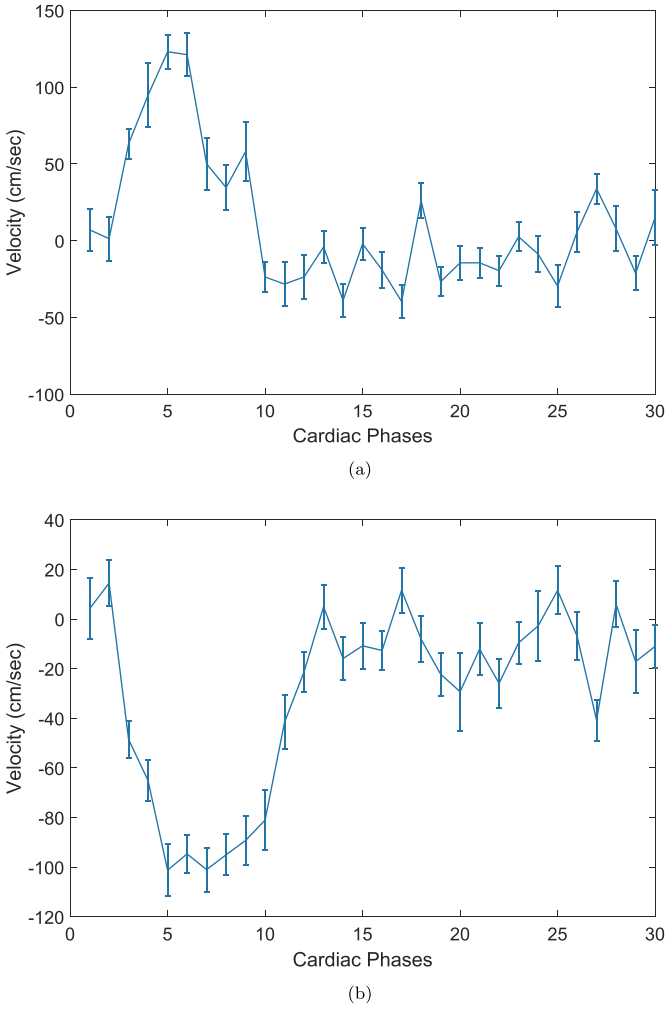

Fig. 8. Velocity and its standard deviation through the cardiac cycle for the (a) ascending and (b) descending aorta, measured in the central pixel.

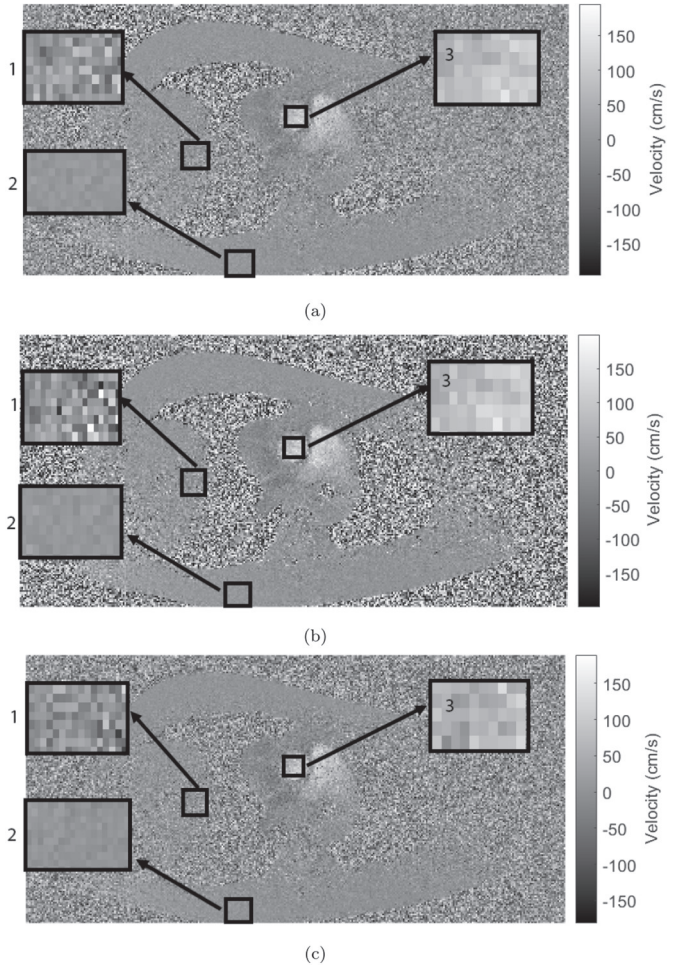

Fig. 9. Velocity in Ascending aorta for one particular time frame, computed from multiple coils with the three methods: (a) WM, (b) SENSE and (c) the proposed VW. Three regions of interest were selected in locations with (1) low, (2) high and (3) moderate SNR values.

4D flow sequence of a single slice with TR/TE = 6.9/4.1 ms for the ascending aorta, TR/TE = 6.9/3.4 ms for the descending aorta, resolution of 1.5 × 1.5 × 4 mm^3, 30 frames per heart beat prospectively gated, and Venc = 200 or 180 cm/s in the ascending and descending aorta respectively. Regarding this data, we only used the through plane velocity.

4. Results

4.1. In-vitro

The phantom data validated the theory. In order to compare the theoretical PDF with the acquired histogram, we used the theoretical continuous Cumulative Distribution Function (CDF) and the empirical CDF. Using the CDF instead of the histogram has several advantages, one of which is avoiding the difficulty of defining the bin size. Fig. 5 shows the CDF for pixels in the background (low SNR), in moderate SNR and in the tube (high SNR). Fig. 5 shows the CDF for the three types of pixels, in all of which there is a good match between the theoretical and experimental functions. In Fig. 5a, we show the case for pixels in the background with a Uniform distribution ($b < 0.7$). In Fig. 5b, we show the case for pixels in relatively low SNR regions ($0.75 < b < 2.3$). In this Figure, an intermediate distribution can be appreciated and also the dependence of the b value, but in all cases, we find good matches. Finally in Fig. 5c, we show the case for pixels in regions of high SNR, and therefore Gaussian distribution ($b > 2.3$). The latter was verified with the One-sample Kolmogorov-Smirnov test. Fig. 6 shows the magnitude (a) and velocity (b) for one particular acquisition. Fig. 6c shows the computed values for b and Fig. 6d the standard deviation for the velocity, evaluated from Fig. 3a. We propose to interpret the velocity in the tube as having a "velocity of 35 ± 5 cm/s".

4.2. In-vivo

We show the results from actual data obtained from the aorta. Fig. 7 shows the values for b (computed with the approximation for a and σ described in Methods), the through plane velocity and the standard deviation of the velocity obtained from the curve in Fig. 3a. These images correspond to the most relevant coils and the time frame when the velocity is at a maximum. As expected, the standard deviation of the velocity is larger for low signal regions and farther away from the coil. From these maps, one can report, for example that the peak velocity in the ascending aorta was 145 ± 15 cm/s. Fig. 8 shows the velocity and its standard deviation for all time frames through the cardiac cycle. Finally, we applied the three methods for combining the velocity from multi-coil data. The results are shown in Fig. 9. We also show three regions selected in places where the SNR is low, moderate and high. The ROI were chosen to include the most similar pixels, such that we can use the spatial standard deviation as a proxy for the standard deviation of the velocity. These standard deviations are shown in Table 1. In the high SNR area all three methods have similar standard deviation

Table 1
Standard deviation (cm/s) for specific areas (Low, High and Moderate SNR) for WM, SENSE and our proposed VW methods.

	Weighted Mean (WM)	SENSE	Our proposed Variance Weighting (VW)
Low SNR ROI (1)	61.1 (cm/s)	84.5 (cm/s)	54.9 (cm/s)
High SNR ROI (2)	9.4 (cm/s)	9.9 (cm/s)	9.7 (cm/s)
Moderate SNR ROI (3)	21.5 (cm/s)	20.6 (cm/s)	24.2 (cm/s)

but in the low SNR area, our method has a reduced standard deviation in comparison with WM and SENSE. In the moderate SNR areas, the SENSE method has less standard deviation values.

5. Discussion

The probability density distribution of the phase of a complex number, given that its components are random variables with a known PDF, is complicated to describe mathematically. That is the case of the velocity computed from an MRI phase-contrast, in the presence of Gaussian noise added to each of the signals channels. Moreover, this probability function changes with the magnitude of the signal, so that the Velocity-to-Noise ratio (VNR) is signal dependent. This was recognized early in the development of MRI phase-contrast, nevertheless today it is common to read that VNR is directly proportional to the Signal-to-Noise ratio (SNR). This proportionality can be misleading if one does not specify that this is in a pixel-based sense. Additionally, this proportionality is only true in the Gaussian regime for the velocity, which in turn is only true for high signal regions.

The noise properties in the MR signal have being extensively studied. See, for example in Ref. [18] and the references therein, where the authors show that in magnitude images the intensity follows a Rician distribution, and consequently there is a bias for low SNR pixels. They also state the analytical formula for the distribution of the phase. For the signal and for the phase they state that there is a threshold in the SNR = 2, above which the distribution is nearly Gaussian. In our study, we take this analysis one step further by adding a convolution in order to reflect the distribution of the difference of the phases; by defining an SNR related value which is spatially variant; and by providing an easy way of computing the true standard deviation, regardless of the SNR.

The purpose of this study is to present, in a unified manner, the true random behavior of the velocity. And more importantly, to show a simple and practical way to estimate its variability. It consists in firstly calculating the parameter b for each pixel, the ratio of the pixel's magnitude to the standard deviation of the acquisition noise. From this b value, one can find the true standard deviation or the probability intervals from the plots in Fig. 3. We encourage everybody working with phase contrast velocity to report some estimation of the precision, such as the standard deviation, together with the computed values.

From the variability analysis in Fig. 3 one can see that for $b > 2.5$ the Gaussian approximation is nearly correct. This happens for pixels where the magnitude of the signal is at least 3.5 times the standard deviation of the noise in each channel. In this case, the standard deviation of the velocity is approximately 0.15 of V_{enc} and there will be a probability of 68% to be in the range ± 15. For lower signal pixels, down to b value of 0.7 ($\sigma \approx 0.45$), or equivalently, when the signal is approximately equal to the standard deviation of the noise, the Gaussian standard deviation is not correct with deviations of up to 10% of the true standard deviation. For pixels with even lower signal levels, the Gaussian approximation is clearly wrong. In this case, it is customary to mask these pixels out, or to weight them by multiplying them with the magnitude. The latter makes sense if one interprets it as dividing the velocity by its standard deviation, which would be the case for the Gaussian approximation.

In our analysis, we made the standard assumptions for velocity reconstruction from phase contrast data, that is, that the velocity is uniform within the voxel; that there is no acceleration or higher order changes in time; and that the duration of the readout is negligible in comparison with the echo time. Any deviation from these assumptions will modify our theoretical results.

The experiments with the simple flow phantom show that the velocity in fact follows the theoretically calculated PDFs, for all SNR levels. The experiment with a volunteer was used as an example of the convenience of using this analysis as opposed to measuring the velocity repeatedly at the cost of lengthening the scan time. Firstly, to show how the variability can be computed and reported, and secondly, to show that knowing the true standard deviation can be used to calculate the optimal weighting for combining the velocity from multiple coils. We show that knowing the precise variability allows to theoretically optimize the variance of the resulting velocity. Previously, it has been studied the advantages of different combination methods. In Ref. [20] , there is a comparison of the Weighted Mean method and the phase obtained by SENSE reconstructed images before computing the phase. That study is mostly experimental and shows that when there is enough SNR both methods are the same, but SENSE is better for lower SNR values, although above 4. Our method, Variance Weighting, is also a weighted mean, but instead of using a proxy for the standard deviation, which is closely related to assuming a Gaussian distribution, we use a true estimation of the variance. The results, shown in Fig. 4, validate the conclusion of Ref. [20] for high SNR but extend the analysis for much lower SNR values, where Variance Weighting is clearly better than WM and SENSE.

6. Conclusion

In this study, we show how to compute the exact probability density function (PDF) of the velocity, obtained with MRI phase-contrast. As expected, for high SNR voxels this PDF is well approximated to a Gaussian distribution. But that is not the case for lesser SNR values. This is important because the velocity is increasingly being used to compute other hemodynamic parameters which are typically more interesting around the boundaries, where the SNR could be reduced. We produce a simple graph from where the validity of the Gaussian hypothesis, and the true standard deviation can be computed from the quotient of the signal value and the signal noise standard deviation. The theoretical values and formulation were validated with experiments in the scanner. Additionally, since we have a good approximation of the standard deviation of the velocity for each coil, we propose a method for combining the multi-coil data in order to minimize the resulting variance of the final velocity. These analyses should help researchers to report the precision of their results when working with phase-contrast velocity.

Declaration of Competing Interest

The authors declare that there is no conflict of interest regarding the publication of this article.

Acknowledgment

The authors acknowledge financial support from: FONDECYT *N°* 3190147, CONICYT-PIA-Anillo ACT1416, FONDECYT *N°* 1191710, and FONDECYT *N°* 1181057. Also, Carlos Sing-Long was partially funded by FONDECYT *N°* 11160728. The Millennium Nucleus for Cardiovascular Magnetic Resonance is supported by the Millennium Scientific Initiative of the Ministry of Economy, Development and Tourism (Chile).

References

[1] Bryant DJ, Payne JA, Firmin DN, Longmore DB. Measurement of flow with NMR imaging using a gradient pulse and phase difference technique. J Comput Assist Tomogr 1984;8(4):588–93.
[2] Dumoulin CL, Souza SP, Walker MF, Wagle W. Three-dimensional phase contrast angiography. Magn Reson Med 1522-25941989;9(1):139–49.
[3] Stankovic Z, Allen BD, Garcia J, Jarvis KB, Markl M. 4D flow imaging with MRI. Cardiovasc Diagn Ther 2014;4(2):173–92.
[4] Zhao M, Charbel FT, Alperin N, Loth F, Clark ME. Improved phase-contrast flow quantification by three-dimensional vessel localization. Magn Reson Imaging 2000;18(6):697–706.
[5] Oyre S, Pedersen EM, Ringgaard S, Boesiger P, Paaske WP. In vivo wall shear stress measured by magnetic resonance velocity mapping in the normal human abdominal aorta. Eur J Vasc Endovasc Surg 1997;13(3):263–71.
[6] et al. Papathanasopoulou P, Zhao S, Kohler U, Robertson MB, Long Q, Hoskins P. MRI measurement of time-resolved wall shear stress vectors in a carotid bifurcation model, and comparison with CFD predictions. J Magn Reson Imaging 2003;17(2):153–62.
[7] Tyszka JM, Laidlaw DH, Asa JW, Silverman JM. Three-dimensional, time-resolved (4D) relative pressure mapping using magnetic resonance imaging. J Magn Reson Imaging 2000;12(2):321–9.
[8] Yang GZ, Kilner PJ, Wood NB, Underwood SR, Firmin DN. Computation of flow pressure fields from magnetic resonance velocity mapping. Magn Reson Med 1522-25941996;36(4):520–6.
[9] Nilsson A, Bloch KM, Carlsson M, Heiberg E, Stahlberg F. Variable velocity encoding in a three-dimensional, three-directional phase contrast sequence: evaluation in phantom and volunteers. J Magn Reson Imaging 2012;36(6):1450–9.
[10] et al. Callaghan FM, Kozor R, Sherrah AG, Vallely M, Celermajer D, Figtree GA. Use of multi-velocity encoding 4D flow MRI to improve quantification of flow patterns in the aorta. J Magn Reson Imaging 2016;43(2):352–63.
[11] Ringgaard S, Oyre SA, Pedersen EM. Arterial MR imaging phase-contrast flow measurement: improvements with varying velocity sensitivity during cardiac cycle. Radiology 2004;232(1):289–94.
[12] Pelc NJ, Herfkens RJ, Shimakawa A, Enzmann DR. Phase contrast cine magnetic resonance imaging. Magn Reson Q 1991;7(4):229–54.
[13] Pelc NJ, Bernstein MA, Shimakawa A, Glover GH. Encoding strategies for three-direction phase-contrast MR imaging of flow. J Magn Reson Imaging 1991;1(4):405–13.
[14] Conturo TE, Smith GD. Signal-to-noise in phase angle reconstruction: dynamic range extension using phase reference offsets. Magn Reson Med 1522-25941990;15(3):420–37.
[15] Andersen AH, Kirsch JE. Analysis of noise in phase contrast mr imaging. Med Phys 2473-42091996;23(6):857–69.
[16] Firoozabadi AD, Irarrazaval P, Uribe S, Tejos C, Sing-Long C. Velocity variability in mri phase-contrast. 2018 26th European Signal Processing Conference (EUSIPCO). 2018. p. 31–5. ISSN 2076-1465.
[17] Davenport WB, Root WL. An introduction to the theory of random signals and noise. 11. 1958. p. 167.
[18] Gudbjartsson H, Patz S. The Rician distribution of noisy MRI data. Magn Reson Med 1995;34(6):910–4.
[19] Thunberg P, Karlsson M, Wigstrom L. Comparison of different methods for combining phase-contrast images obtained with multiple coils. Magn Reson Imaging 2005;23(7):795–9.
[20] Lu K, Liu TT, Bydder M. Optimal phase difference reconstruction: comparison of two methods. Magn. Reson. Imaging 0730-725X2008;26(1):142–5.
[21] Pruessmann KP, Weiger M, Scheidegger MB, Boesiger P. SENSE: sensitivity encoding for fast MRI. Magn Reson Med 1999;42(5):952–62.
[22] Bydder M, Larkman DJ, Hajnal JV. Combination of signals from array coils using image-based estimation of coil sensitivity profiles. Magn Reson Med 2002;47(3):539–48.